redin Revista Facultad de Ingeniería, Universidad de Antioquia, No.107, pp. 39-52, Apr-Jun 2023

# Numerical analysis of soil desaturation by an air injection method

## Análisis numérico de desaturación del suelo mediante un método de inyección de aire

**Sebastián Sepúlveda-Cano** [1], **Carlos A. Vega-Posada** [1], **Edwin F. García-Aristizábal** [1*]

[1]Escuela Ambiental, Universidad de Antioquia. Calle 67 # 53-108. A. A. 1226. Medellín, Colombia.

**CITE THIS ARTICLE AS:**

S. Sepúlveda-Cano, C. A. Vega-Posada and E. F. García-Artistizábal. "Numerical analysis of soil desaturation by an air injection method", *Revista Facultad de Ingeniería Universidad de Antioquia*, no. 107, pp. 39-52, Apr-Jun 2023. [Online]. Available: https://www.doi.org/10.17533/udea.redin.20220580

**ARTICLE INFO:**

Received: March 26, 2021
Accepted: May 15, 2022
Available online: May 16, 2022

**KEYWORDS:**

Ground improvement; liquefaction; soil desaturation; numerical analysis

Mejoramiento de suelo; licuefacción; desaturación del suelo; análisis numérico

**ABSTRACT:** A numerical analysis is conducted to evaluate the effective radius of air advance ($R_{eff}$) in coarse-grained, saturated, sandy deposits improved by means of air injection (i.e., soil desaturation). It is well-known that the cyclic resistance to liquefaction of a saturated sandy deposit is highly affected by the presence of gas in the void space. A parametric study is performed to investigate the soil's main hydraulic parameters and air-injection conditions of the transient gas affecting $R_{eff}$ and controlling the desaturation process. The effects of the a) soil-water characteristic curve, b) intrinsic permeability, c) injection pressure, and d) duration of air injection are investigated. It is shown that the injection pressure and soil's intrinsic permeability are the main factors influencing the extent of $R_{eff}$. The analysed cases showed that, for a fixed injection pressure, the soil will achieve a maximum value for $R_{eff}$. This threshold value is reached more rapidly when the soil's intrinsic permeability increases. The results aim to shorten existing knowledge gaps and contribute to the development of design methodologies for air-injection desaturation techniques.

**RESUMEN:** Se realiza un análisis numérico para evaluar el radio efectivo de avance del aire ($R_{eff}$) en depósitos arenosos saturados de grano grueso mejorados mediante inyección de aire (es decir, desaturación del suelo). Es bien sabido que la resistencia cíclica a la licuefacción de un depósito arenoso saturado se ve muy afectada por la presencia de gas en espacios vacíos. Se realiza un estudio paramétrico para investigar los principales parámetros hidráulicos del suelo y las condiciones transitorias de inyección del aire que afecta a $R_{eff}$ y controla el proceso de desaturación. Se investigan los efectos de a) la curva característica suelo-agua, b) la permeabilidad intrínseca, c) la presión de inyección y d) la duración de la inyección de aire. Se muestra que la presión de inyección y la permeabilidad intrínseca del suelo son los principales factores que influyen en la extensión de $R_{eff}$. Los casos analizados mostraron que, para una presión de inyección fija, el suelo alcanzará un valor máximo de $R_{eff}$. Este valor límite se alcanza más rápidamente cuando aumenta la permeabilidad intrínseca del suelo. Los resultados tienen como objetivo reducir las lagunas de conocimiento existentes y contribuir al desarrollo de metodologías de diseño para técnicas de desaturación por inyección de aire.

* Corresponding author: Edwin F. García-Aristizábal
E-mail: edwin.garcia@udea.edu.co
ISSN 0120-6230
e-ISSN 2422-2844



DOI: 10.17533/udea.redin.20220580

**List of notations**

| | |
|---|---|
| $R_{eff}$ | effective radius of air advance |
| $\theta$ | total porosity |
| $S_i$ | degree of saturation phase $i$ |
| $i$ | Phase ($w$ for the wetting phase and $nw$ for the non-wetting phase) |
| $t$ | time |
| $k_{int}$ | intrinsic permeability |
| $k_{r,i}$ | relative permeability phase $i$ |
| $\mu_i$ | fluid´s dynamic viscosity phase $i$ |
| $\rho_i$ | fluid density phase $i$ |
| $P_c$ | capillary pressure |
| $S_{max}$ | maximum degree of saturation |
| $S_{min}$ | minimum degree of saturation |
| $a$ | shape parameter |
| $b$ | shape parameter |
| $n$ | material parameter |
| $m$ | material parameter |

# 1. Introduction

Liquefaction is a well-known phenomenon in the geotechnical community. It is commonly associated with the loss of shear strength in saturated, sandy soil deposits subjected to dynamic loads such as those experienced during an earthquake. A description of available soil improvement methods to mitigate liquefaction is provided by Seed *et al.* [1]. In general, these ground improvement techniques are expensive and only applied to sensitive and large projects [2]. Therefore, there is a manifest necessity for developing inexpensive, cost-effective mitigation methods that can be easily implemented for new and existing structures [3]. The geotechnical community has discussed the possibility of soil desaturation as a technique to improve the soil's cyclic shear resistance [4]. For this purpose, several techniques have been proposed and tested to introduce occluded gas bubbles into the saturated soil medium. When the soil is subjected to a cyclic load, the gas absorbs the induced pore pressure by reducing its volume and, as a consequence, decreases the soil's susceptibility to liquefaction [5]. Among these techniques are a) air injection [4], b) water electrolysis [6], c) chemical reactions [7], d) microbiological processes [8] and e) drainage-recharge [6]. Bubble generation methods offer a less invasive alternative in comparison to other methods commonly used, cost-effective, and practical when soil improvement is considered difficult (i.e., it could affect the stability of existing structures) [9]. In this work, a mathematical formulation is presented to estimate changes in the degree of saturation of the soil, $S(\%)$, during air injection. Slight decreases in $S(\%)$ will substantially increase the soil's cyclic shear resistance. A parametric analysis is performed to evaluate the effects of the soil-water characteristic curve, permeability functions, pressure injection, and injection time on $R_{eff}$. In the numerical analysis, the standard mechanisms of a biphasic flow are included (i.e., incompressible and isothermal flow in an isotropic homogeneous porous media). In order to perform the simulations, the lite (free) version of the PDE Solutions Inc [10] software was used. This is a commercially available toolkit that provides state-of-the-art solution methods for numerically solving partial differential equations.

The desaturation process for liquefaction mitigation is still a relatively new approach, and it needs to be investigated for future applications. Several aspects such as (1) induced degree of saturation, (2) distribution and homogeneity of gas bubbles, (3) longevity of gas bubbles, and (4) desaturation plume extension need to be addressed in further detail. The present work is carried out with the objective of contributing to the state of the art on techniques dealing with liquefaction mitigation of coarse-grained, saturated, sandy soils by means of air injection. The results aim to shorten existing knowledge gaps regarding the mechanical processes controlling the extension of the desaturation plume and promote the development of design methodologies for air-injection desaturation techniques.

# 2. Analysis and simulation of gas injection into a saturated porous material

## 2.1 Mathematical model

Air injection in a saturated porous media is treated as a biphasic flow problem. Herein, the mathematical formulae presented by Pinder and Gray [11], which are based on the work conducted by Darcy [12], are implemented in the proposed mathematical model. Considering a porous medium biphasic flow, the macro-scale balance equation for air (non-wetting phase, *nw*) and water (wetting phase, *w*) phases are as follows:

$$\theta\frac{\partial S_w}{\partial t}+\nabla\cdot\left[-\frac{k_{\text{int}}\,k_{r,w}}{\mu_w}\left(\nabla p_w+\rho_w g\nabla D\right)\right]=0 \quad (1)$$

$$\theta\frac{\partial S_w}{\partial t}+\nabla\cdot\left[-\frac{k_{\text{int}}\,k_{r,nw}}{\mu_{nw}}\left(\nabla p_{nw}+\rho n_w g\nabla D\right)\right]=0 \quad (2)$$

Where $\theta$ is the total porosity; $S_i$ is the degree of saturation; t is time; $k_{int}$ is the intrinsic permeability of the material ($m^2$); $k_{r,i}$ is the relative permeability associated to the fluid *i*; $\mu_i$ is the fluid's dynamic viscosity (*Pa s*); $p_i$ is the fluid pressure (*Pa*); ρi is the fluid density (kg/$m^3$); *g* is the acceleration of gravity; and *D* is the coordinate of vertical elevation (*m*). In these definitions, subscript $i = w$ for the wetting phase and $i = nw$ for the non-wetting phase. The

saturation of the phases can be expressed by the following constitutive expression:

$$S_w + S_{nw} = 1 \tag{3}$$

This expression is an extension of Darcy's law to a two-phase flow. The macro-scale capillary pressure ($p_c$) can be defined as:

$$p_c = p_{nw} - p_w \tag{4}$$

The above expressions simplify Equations (1) and (2) by eliminating two unknowns, and the conservation of mass equation of the pore fluid is then only dependent on $p_{nw}$ and $S_{nw}$. Since capillary pressure is governed by $S_w$, the capillary term, $\nabla p_c$, can be expressed as:

$$\nabla p_c = \frac{\partial p_c}{\partial S_w} \nabla S_w \tag{5}$$

Substituting Equations (3), (4), and (5) into Equation (1) and adding Equation (2), the system of conservation of mass is written in a pressure-saturation form and expressed in Equations (6) and (7), respectively, as:

$$\left[ -\frac{k_{int} k_{r,w}}{\mu_w} \left( \nabla p_{nw} + \rho_w g \nabla D - \frac{\partial p_c}{\partial S_w} \nabla S_w \right) - \frac{k_{int} k_{r,nw}}{\mu_{nw}} \left( \nabla p_{nw} + \rho_{nw} g \nabla D \right) \right] = 0 \tag{6}$$

$$\theta \frac{\partial S_{nw}}{\partial t} + \nabla \cdot \left[ -\frac{k_{int} k_{r,nw}}{\mu_{nw}} \left( \nabla p_{nw} + \rho_{nw} g \nabla D \right) \right] = 0 \tag{7}$$

From the hydraulic properties of unsaturated soils, the effective degree of saturation of the $w$ phase is given by Equation (8):

$$S_{w,eff} = \left( \frac{S_w - S_{\min}}{S_{\max} - S_{\min}} \right) \tag{8}$$

where $S_{max}$ and $S_{min}$ are the maximum and minimum limiting values of $S_w$, respectively. The relative permeability of the water and air phases are given by Equations (9) and (10), respectively.

$$k_{r,w} = S_{w,eff}^{a} \left[ 1 - \left( 1 - (S_{w,eff})^{\frac{1}{m}} \right)^{m} \right]^2 \tag{9}$$

$$k_{r,nw} = (1 - S_{w,eff})^{b} \left( 1 - (S_{w,eff})^{\frac{1}{m}} \right)^{2m} \tag{10}$$

where $a$ and *b* are the shape parameters and *m* a material parameter. Now, the van Genuchten [13] expression for the soil-water characteristic curve is given by Equation (11):

$$p_c = \frac{1}{\alpha} \left( S_{w,eff} \frac{-1}{m} - 1 \right)^{1-m} \tag{11}$$

where $m$ and $n$ are material parameters and $m = 1 - (1/n)$. Deriving Equation (11), the capillary term in Equation (6) is expressed as follows (equivalent to the work of Horgue *et al.* [14]):

$$\frac{\partial p_c}{\partial S_w} = -\frac{1-m}{\alpha m} \left( (S_{w,eff})^{\frac{-1}{m}} - 1 \right)^{-m} (S_{w,eff})^{-\frac{1+m}{m}} \tag{12}$$

## 2.2 Validation of the proposed model

Yasuhara *et al.* [15] carried out an experimental program to induce, by means of air injection, a partial degree of saturation in a fully saturated soil column. He also conducted a numerical analysis to validate the experimental results. Nominal flow rates and the induced partial degree of saturation were recorded. Figure 1 shows a sketch of the acrylic box and instrumentation set-up implemented to conduct the desaturation process. It consists of a transparent acrylic box 1.72 *m* long, 0.90 *m* high, and 0.60 *m* width containing a fully saturated homogeneous column test of Toyoura Sand with $D_r = 60$ % and $e_0 = 0.755$. The test was developed under conditions that allowed a) flow of water and air at the top of the column, b) a hydrostatic pressure distribution for the initial wetting phase, and c) air injection into the saturated soil medium throughout an inlet port placed at the centre-bottom of the box.

The experimental and numerical results reported by Yasuhara *et al.* [15] are used to validate the mathematical formulation and numerical analysis proposed in the present work. Similar soil parameters, injection pressures, and boundary conditions as those used by Yasuhara *et al.* [15] in their simulations are adopted for the numerical analysis. Figure 1 represents the rectangular area selected for the Finite Element analysis (half of the domain). Table 1 lists the material input parameters used for analysis.

Figure 2 shows the comparison between the experimental and numerical results from Yasuhara *et al.* [15] with the proposed numerical analysis for changes in the degree of saturation of the wetting phases ($S_w$). Locations A, B, C, and D have coordinates ($x$ and $y$) inside the domain equal to (0.86,0.32), (0.65,0.32), (0.545,0.32) and (0.44,0.32), respectively. A significant discrepancy between the experimental results and both numerical analyses (i.e., the proposed approach and Yasuhara's numerical formulation) is observed. Yasuhara *et al.* [15] addressed these discrepancies and they were mainly attributed to differences between the real and measured soil physical properties (e.g., permeabilities and the soil-water characteristic curve) and the equations that represent the phenomena. On the other hand, and as presented in Figure 2b, the comparison between the numerical results shows a good agreement. Figure 2b shows a time delay on $S_w$ at locations A, B, C, and D. This lag in advance of the non-wetting phase front can be primarily explained by the uncertainties associated with the methodologies concerning the numerical models and relative permeability functions. These parameters are directly related to the soil's initial void ratio and experimental work, and they are part of the 3D model formulation solved with the integral finite difference

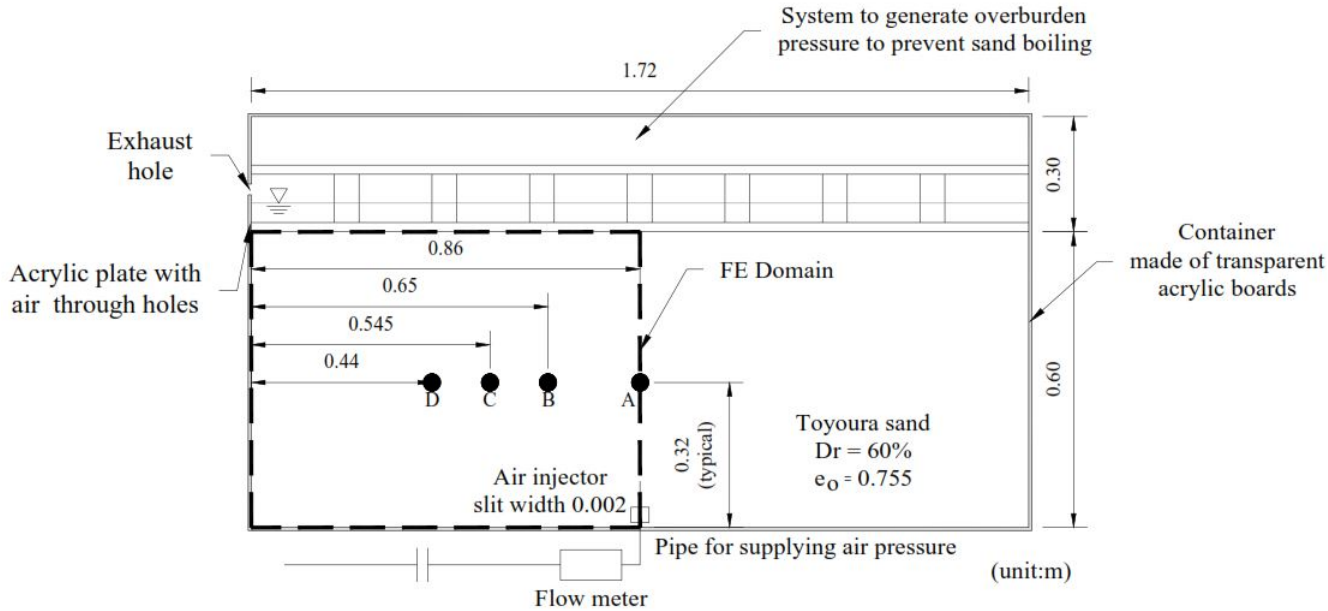


**Figure 1** Sketch of the transparent acrylic box. Values of Sw were measured at locations A, B, C and D. Modified from Yasuhara *et al.* [15]

**Table 1** Material and hydraulic parameters used for numerical simulations

| Variable | Value | Description |
|---|---|---|
| $\rho_w$ | 1000 $kg/m^3$ | Fluid density, wetting phase |
| $\mu_w$ | $1x10^{(-3)}Pas$ | Dynamic viscosity, wetting phase |
| $\rho_{nw}$ | 1.28 $kg/m^3$ | Fluid density, non-wetting phase |
| $\mu_{nw}$ | $1.81x10^{(-5)}Pas$ | Dynamic viscosity, non-wetting phase |
| $\theta$ | 0.421 | Porosity |
| $S_max$ | 1.0 | Maximum degree of saturation, wetting phase |
| $\alpha$ | $2.237x10^{(-4)}1/Pa$ | Van Genuchten $\alpha$ parameter |
| $n$ | 8.696 | Van Genuchten *n* material parameter |
| $a$ | 0.50 | Shape parameter, wetting phase |
| $b$ | 0.33 | Shape parameter, non-wetting phase |
| $k_{int}$ | $2.04x10^{(-11)}m^2$ | Intrinsic permeability |

method proposed by Yasuhara *et al.* [15]. The following trends are observed when comparing both numerical simulations: (1) $S_w$ initially decreases near the injector and progressively around the soil column as air infiltrates due to buoyancy and the induced pressure gradients in the non-wetting phase, (2) $S_w$ starts to decrease at a later stage, but it shows a similar tendency on the desaturation process as well as a similar minimal value of $S_w$ at the end of the injection process ($t = 5,500s$), and (3) After $t = 5,500s$, $S_w$ begins to increase due to the shutdown of the air injector; nonetheless, a non-wetting phase still remains inside the domain resulting in $S_w$ values less than 0.9 at $t = 6,000s$. The reduction in $S_w$ after the shutdown may also be attributed to the escape of excess air bubbles from the void spaces due to buoyancy forces.

In the proposed analysis, the advance of the air front is controlled only by hydraulic factors, especially by the amount of pore fluid flow crossing the medium. This pore fluid flow is generated by the non-wetting phase pressure gradients associated with diffusion (conduction) and not by the transport of air dissolved by advection and dispersion. The proposed model does not consider the effects of the non-wetting phase compressibility, which can influence the hydraulic response of the soil due to the permeability and pressure dependency. Thus, from the simulations, it is observed that the biphasic flow implemented in the proposed FE model captures the general trends shown by Yasuhara *et al.* [15].

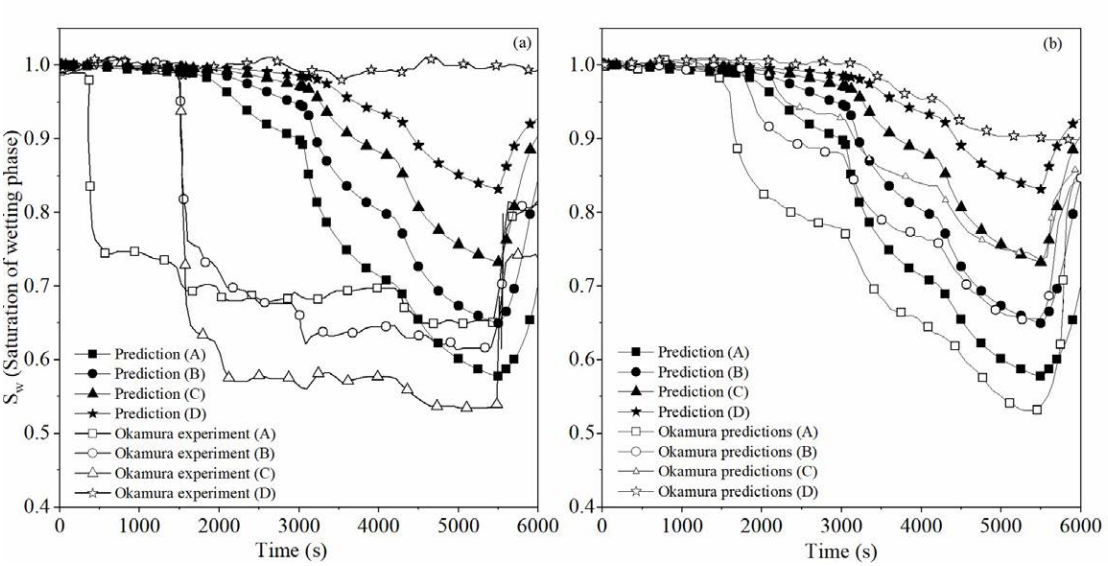


**Figure 2** Comparison between the present work and Yasuhara's predictions of Sw

# 3. Results and discussion

## 3.1 Parametric analysis of air injection

In order to carry out decontamination processes of saturated soils, different studies related to air sparging have been conducted, in which the effect of soil parameters [16], the mechanisms of mass transfer [17], air migration [18], systems and implementation [19], predictive modelling [20] and the performance assessment [21] have been studied. However, the lack of studies focused on soil desaturation processes as a mechanism for liquefaction mitigation is apparent. Next, a parametric analysis is conducted to study the evolution of soil desaturation by air injection. Predictions of the desaturation radius and distributions in time and space of $S_w$ are evaluated via a multiphase flow simulation. Since the induce of partial saturation as a countermeasure technique for soil liquefaction is a relatively new approach, and there is not yet a well-established methodology, the results presented herein may be of great interest to engineers dealing with soil desaturation techniques.

This parametric study is conducted to evaluate the influence of the hydraulic parameters ($\alpha$, $n$, $a$, and $b$) and injection pressures on $R_{eff}$. The hydraulic parameters were selected from Lu and Likos [22], and they are listed in Tables 2 and 3. These parameters are considered representative of sands and silty sand soils. In Table 2, underlined values are kept invariant while a group of predictions is generated. For instance, to study the influence of parameter *n*, the underlined values of $\alpha = 0.10(1/kPa)$, $S_{w,max} = 1.0$, $a = 3.0$, $b = 0.33$, $k_{int} = 1.00x10^{-11}m^2$, and $P_{nw,inj} = 90kPa$ are kept constant while varying *n*. The same approach is conducted to study the influence of the other parameters. A second group of simulations is conducted on four different soil types and analysed for air injection pressures varying from 70 to 100 *kPa* (Table 3). Material parameters listed in Table 3 are representative of different silty sands $\alpha = 0.07(1/kPa)$ and $n = 2.0$; 0.10 *1/kPa* and *n* =4.0) and sandy soils $\alpha = 0.12(1/kPa)$ and *n* =6.0; 0.14 *1/kPa* and *n* =8.0). Each soil in Table 3 has an associated intrinsic permeability and hydraulic parameters that are dependent only on the pore size, pore geometry, and pore size distribution. Intrinsic permeability is identical for any soil regardless of the type of characteristics of the fluid being conducted on the assumption that the pore structure remains unaltered. Note that intrinsic permeability can fluctuate several orders of magnitude for the same nominal soil type; consequently, a range of intrinsic permeability values was selected to represent a variety of pervious and semi-pervious soils ranging from clean to very fine sands with high silt content.

Table 4 shows the values used for the physical properties of both air and water. Data from Chen *et al.* [23]. Figure 3 depicts the FE model domain used for analysis. The model consists of a homogeneous soil with dimensions of 30 *m* in width and 15 *m* in depth. For the non-wetting phase, a no-flow boundary condition is assigned to the bottom of the model and to the borehole for air injection. A non-wetting flow is allowed to the rest of the boundaries as well as to the point where the injector is located (i.e., 6.0 *m*). The simulations began from a fully wetting phase condition (i.e., saturated condition), and the non-wetting phase began to flow as the pressure generated at the injector overcomes the hydrostatic pressure. The isocountors

presented in all of the following figures correspond to de advance of the no wetting phase ($S_{nw}$), and they are generated from a fixed zoom with an 8.8 *m* square shape. The left lower edge of the zoom is located at coordinates $x$= 10.6 $m$ and $y = 7.2m$. Figure 3 encloses, with dashed lines, the square area associated with the zoom.

## Results and discussion of numerical simulations for the first parametric study

### Effects of injection pressure

Figure 4 shows the time-space variation of $S_{nw}$ as a function of injection pressure and for injection times from $900s$ to $3,600s$ for the underlined values listed in Table 2. In total, six injection pressures were implemented for analysis, but only four are presented for the sake of simplicity.

The first four injection pressures ($P_{nw,inj}$=70, 75, 80, and 85 $kPa$) are less than the maximum injection pressure suggested by Ogata and Okamura [24] for soil desaturation purposes. Ogata and Okamura [24] recommended $\sigma_{\text{jni.max}} = \sigma_{hyd} + 0.5\sigma'_v$, so that the soil skeleton is not disturbed during air injection. In the present analysis, the maximum injection pressure is equivalent to 87 $kPa$ (for an injector located at 6.0 m and a soil with $\gamma = 19.0kN/m^3$). The sixth injection pressure ($P_{nw,inj} = 100kPa$) is higher than that recommended by Ogata and Okamura [24] and it could induce rearrangement of the internal structure of the soil to be improved [25]. However, this value of $P_{nw,inj}$ was analysed with the main objective of establishing whether the advance of the desaturation front has a response that is directly proportional to the increase in injection pressure or if it exhibits a different trend.

It is clearly observed in Figure 4 how, as injection pressure increases, the soil changes from an initially entire saturated condition to a partially saturated state. Because at *t=3,600 s* the non-wetting phase (air phase) has not yet reached the drained boundaries, the volumetric content of the displaced water phase (air phase) is the same as the volumetric content of injected non-wetting phase (since equations represent an incompressible flow). A non-wetting phase infiltrating into the saturated soil results in a decrease in $S_w$. Furthermore, if the pressure at which the non-wetting phase is injected increases, there will be a more significant air front advance and a more predominant vertical advance of the non-wetting phase (i.e., due to gravitational forces).

Figure 5 presents the $R_{eff}$ associated with the isocountors shown in Figure 4, corresponding to $S_{nw} = 0.1$ and $P_{nw,inj}$ ranging from 70 to 100 $kPa$. The value of $S_{nw} = 0.1$ was selected because, as shown by Chaney [26] and Yoshimi *et al.* [27], the liquefaction susceptibility of fully saturated sands decreases by half when the degree of saturation of the soil is reduced by 10 %. As expected, it is observed that the higher the injection pressure, the greater the effective radius of $S_{nw}$. Okamura *et al.* [28] observed a similar trend in an in-situ monitoring desaturation program of a three-dimensional layered soil column. For a fixed time, it can be seen that $R_{eff}$ varies significantly with variations in $P_{nw,inj}$. For the analysed case (silty sand), $R_{eff}$ increases by approximately 3 times when $P_{nw,inj}$ increases from 70 to 100 $kPa$. For a fixed injection pressure, the increase in $R_{eff}$ is more pronounced at the beginning of the desaturation process and it becomes less marked as time advances. As shown later, the soil reaches a maximum $R_{eff}$ for a given injection pressure.

### Influence of parameters $\alpha$, n, a, and b

Figure 6 shows the influence of material parameters $\alpha$, *n*, $a$, and *b* on the predicted $R_{eff}$. For a constant permeability and injection pressure, material parameters $\alpha$ and *n* (van Genuchten parameters) have a more significant influence than parameters $a$ and *b* (Shape parameters) on $R_{eff}$. For the case of parameter $\alpha$, $R_{eff}$ slightly increases as $\alpha$ increases. This response is anticipated since higher values of parameter $\alpha$ represent coarse-grained soils (sands). On the other hand, material parameter $n$ has a more complex influence (nonlinear response) on the extent to which the material is partially desaturated. Initially, and for the same injection pressure and permeability, $R_{eff}$ remains almost constant with time when *n*=1.3 and it grows very rapidly when $n$ increases from 1.3 to 2.0. For values of $n$ between 2.0 and 4.0, $R_{eff}$ still increases but at a slightly slower rate. Similar behaviour is observed when n increases from 4.0 to 8.0 but with a tendency to become constant as $n$ increases. Higher values of $n$ (sands) represent a more rapid transition between saturated and unsaturated conditions. Material parameters *a* and *b* do not have a significant influence on the partial degree of saturation achieved during air injection. Table 5 summarizes the results of $R_{eff}$ for the first set of simulations. The values are taken at *t*=3,600 *s*. $R_{eff}/R_0$ corresponds to the ratio between the calculated effective radius of the variable being considered and the effective radius of the first assumed value (underlined in Table 5). The numerical results show some general trends in the value of $R_{eff}$ that could potentially be used to develop soil desaturation methodologies. For instance, and for practical purposes, higher values of $R_{eff}$ are reflected in greater separation between the injection wells during a soil desaturation process.

For a fixed intrinsic permeability, $k_{int} = 1.00x10^{-11}$ $m^2$, $R_{eff}$ increases by a factor of 2.89 when the injection pressure increases from 70 to 100 *kPa*, highlighting the

**Table 2** Hydraulic parameters, injection pressures, and permeability used for the first parametric study

| $\alpha(1/kPa)$ | $n$ | $s_{w,max}$ | $a$ | $b$ | $P_{nw,inj}(kPa)$ | $k_{int}(m^2)$ |
|---|---|---|---|---|---|---|
| 0.07 | 1.30 | 1.00 | 0.50 | **0.33** | 70 | $1.00x10^{-11}$ |
| 0.10 | 2.0 | | 1.0 | 0.50 | 75<br>80<br>85 | |
| 0.12 | **4.00** | | 2.0 | 0.80 | **90** | |
| 0.14 | 8.00 | | **3.00** | 1.00 | 100 | |

**Table 3** Hydraulic parameters, injection pressures, and permeabilities used for the second group of simulations

| **Soil** | $\alpha(1/kPa)$ | $a$ | $b$ | $n$ | $k_{int}(m^2)$ |
|---|---|---|---|---|---|
| 1 | 0.07 | 3.00 | 0.33 | 2.0 | $5.55x10^{-12}$ |
| 2 | 0.10 | | | 4.0 | $1.00x10^{-11}$ |
| 3 | 0.12 | | | 6.0 | $5.55x10^{-11}$ |
| 4 | 0.14 | | | 8.0 | $1.00x10^{-10}$ |

$P_{nw,inj} = 70, 75, 80, 85, 90$ and $100kPa$

**Table 4** Material parameters used for simulations

| **Variable** | **Value** | **Description** |
|---|---|---|
| $\rho_w$ | 1000 $kg/m^3$ | Fluid density, wetting phase |
| $\mu_2$ | $1x10^{-3}Pas$ | Dynamic viscosity, wetting phase |
| $\rho_{nw}$ | 1.28 $kg/m^3$ | Fluid density, non-wetting phase |
| $\mu_{nw}$ | $1.81x10^{-5}Pas$ | Dynamic viscosity, non-wetting phase |
| $\theta$ | 0.34 | porosity |
| $S_{w,max}$ | 1.0 | Maximum degree of saturation, wetting phase |
| $S_{w,min}$ | 0.0 | Minimum degree of saturation, wetting phase |

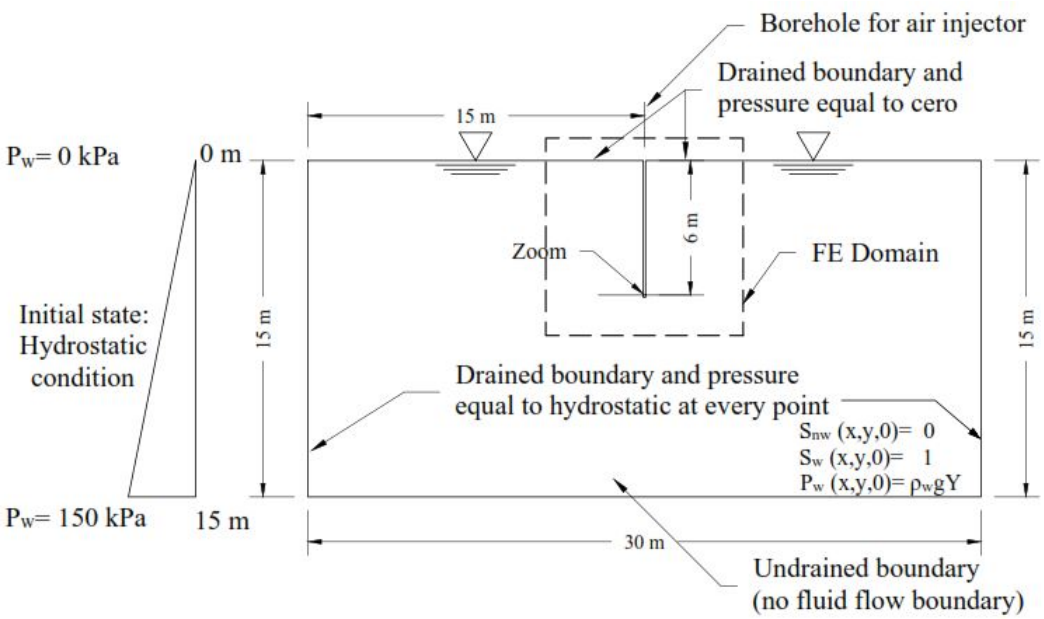


**Figure 3** FE domain and boundary conditions of the proposed model

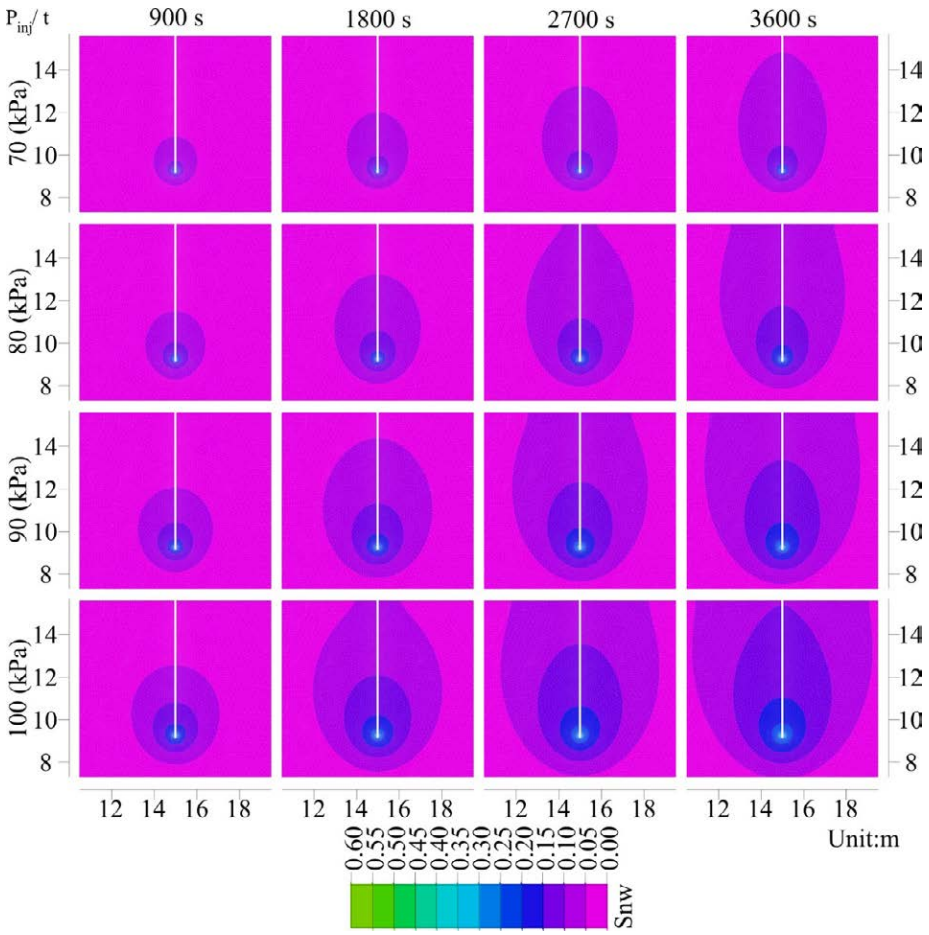


**Figure 4** Isocountors-distribution of $S_{nw}$ due to changes in $P_{nw,inj}$. Distance in meters

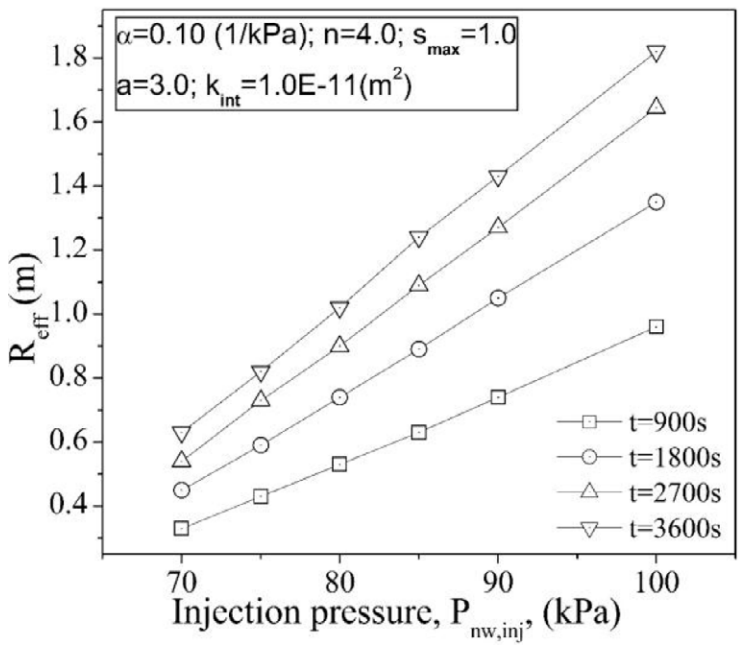


**Figure 5** $R_{eff}$ from the isocontours. $S_{nw} = 0.1$

importance of the magnitude of injection pressure on the extent of the desaturation zone. With regards to the water retention characteristic curve parameters ($\alpha$ and *n*), it is observed that $R_{eff}$ increases only by 1.09 times when α increases from 0.07 to 0.14; meanwhile, if parameter *n* increases from 1.3 to 8.0, $R_{eff}$ increases by 5.10 times. This implies that the shape of the soil-water retention characteristic curve has a more significant influence on the advance of the desaturation front. Because $\alpha$ is related to the inverse of the soil air entry value, soils with lower air entry values (soils with larger particles and pore sizes) will allow a more rapid desaturation process since air enters the soil more freely.

On the other hand, a significant increase in $R_{eff}$ is observed when *n* becomes larger. Parameter *n* captures the pore size distribution within the soil, being higher for soils with bigger particles and pore sizes. This implies that the desaturation process will be more effective in soils with larger particles. Because the air injection process induces a partially saturated condition within the soil, knowledge of the water retention characteristic curve is fundamental for developing a design methodology and making the desaturation process more effective. In addition, slight variations in $R_{eff}$ are observed when the permeability function parameters are analysed (*a* and *b* parameters), suggesting that these parameters do not have a relevant influence on the desaturation process. This is probably because the desaturation levels achieved during air injection are low and the variation in permeability is minimal.

## Results and discussion of numerical simulations for the second parametric study

Table 3 presents the set of parameters studied to observe the effect of intrinsic permeability and injection pressures on the non-wetting phase flow and $R_{eff}$. Figure 7 shows the isocountors of the predicted evolution of $S_{nw}$ as a function of the injection pressure and intrinsic permeability. For the sake of simplicity, only injection pressures of 70, 80 and 90 *kPa* at *t*=1,800 *s* are presented. It is observed that, for a particular injection pressure, the more permeable the soil, the greater the infiltration of the non-wetting phase front; in other words, the higher the advance of the desaturation plume within the saturated soil medium. Also, the higher the pressure at which the non-wetting phase is injected, the more pronounced the vertical advance of this phase. Typically, in the predictions, the desaturation plume has a cone or parabolic shape similar to that presented by Nyer and Suthersan [29] and Chen *et al.* [30], respectively. As observed in the results, and as stated by Reddy *et al.* [31], the dimensions of the desaturation plume are substantially dependent on the soil characteristics, injection pressures, and depth of the injector (hydrostatic pressure to overcome). Figure 8 shows the effective radius profiles associated with the hydraulic parameters, soil permeabilities, and pressure injections listed in Table 3. The readings were taken at times equal to 900 *s*, 1,800 *s*, 2,700 *s*, and 3,600 *s*. Figure 8a presents the values of $R_{eff}$ for the soil with $k_{int}$= $5.55x10^{-12}$ $m^2$. For all pressures, $R_{eff}$ gradually increases with time and the effect is more pronounced at higher injection pressures and at the early stages of the desaturation process. It is observed that regardless of the injection pressure, the rate of increase in $R_{eff}$ is less as injection time increases, suggesting that the soil is achieving a maximum $R_{eff}$ for the applied pressure. Figure 8b shows $R_{eff}$ for the soil with $k_{int}$= $1.00x10^{-11}$ $m^2$. This soil has an intrinsic permeability half order of magnitude higher than the soil in Figure 8a. A similar response is observed between these two soils. Figures 8c and 8d show $R_{eff}$ for two most permeable soils ($k_{int}$= $5.55x10^{-11}$ $m^2$ and $1.00x10^{-10}m^2$). Similar to the least permeable soils, $R_{eff}$ increases with time as the injection pressure increases, and for a given pressure, the soil reaches an apparent state of equilibrium.

Additionally, from Figures 8c and 8d, it is noticed that a maximum $R_{eff}$ is reached for all injection pressures at the early stages of the desaturation process (*t*=900 *s* and *t*=1,800 *s*, *respectively*). This trend suggests the existence of a maximum $R_{eff}$ for a given injection pressure level, which is reached more rapidly as the soil's intrinsic permeability increases. This state of equilibrium in the degree of saturation of the non-wetting phase is primarily the result of a steady-state flow condition reached during the air injection process.

Figure 9 shows $R_{eff}$ as a function of permeability and injection pressure. It is observed that at lower values of intrinsic permeabilities, $k_{int} = 5.55x10^{-12}m^2$ and $1.00x10^{-11}m^2$, $R_{eff}$ grows almost linearly with increments in injection pressure. For the most permeable soils, $k_{int} = 5.55x10^{-11}m^2$ and $1.00x10^{-10}m^2$, the trend is similar, but the increase in $R_{eff}$ is more pronounced as pressure increases. Both permeable soils achieved a similar $R_{eff}$ regardless of injection pressure.

Table 6 summarizes the results of $R_{eff}$ obtained for the second group of simulations (Table 3). It is noticed that $R_{eff}/R_0$ becomes larger as the intrinsic permeability increases. For instance, $R_{eff}$ increases 2.40 times when $k_{int}$ increases one order of magnitude (from $k_{int} = 5.5x10^{-12}$ to $k_{int} = 5.5x10^{-11}$), implying that air injection processes are more effective and faster in soils with higher saturated intrinsic permeabilities. Soils 3 and 4 reached the same $R_{eff}$, indicating that there is a threshold intrinsic permeability value where no major increases in $R_{eff}$ are obtained. These results highlight the importance of the intrinsic permeability on the extent

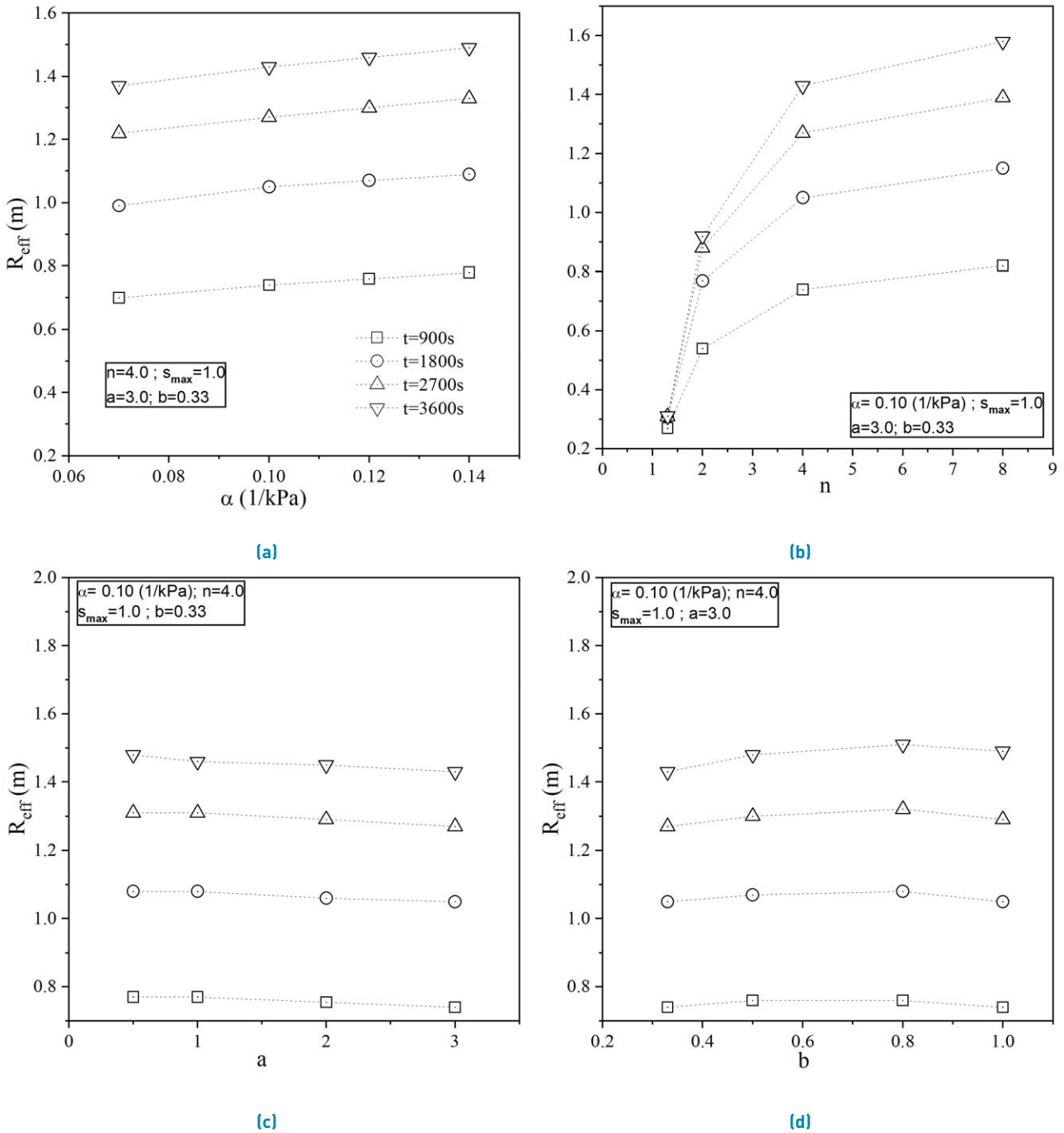


**Figure 6** Predicted $R_{eff}$ as a function of $\alpha$, *n*, *a* and *b*. $S_{nw}$=0.1, $P_{nw,inj}$=90 *kPa*, and $k_int = 1.0x10^{-11}(m^2)$

**Table 5** Summary of results obtained for $R_eff$ as a function of $P_{nw,inj}$ and $\alpha$, *n*, *a*, and *b* parameters. $k_{int} = 1.0x10^{-11}(m^2)$

| $P_{nw,inj}$(kPa) | $R_{eff}$ (m) | $R_{eff}/R_0$ | $\alpha$ (1/kPa) | $R_{eff}$ (m) | $R_{eff}/R_0$ | *n* | $R_{eff}$ (m) | $R_{eff}/R_0$ |
|---|---|---|---|---|---|---|---|---|
| 70 | **0.63** | 1.00 | 0.07 | **1.37** | 1.00 | 1.30 | **0.31** | 1.00 |
| 80 | 1.02 | 1.62 | 0.10 | 1.43 | 1.04 | 2.00 | 0.92 | 2.97 |
| 90 | 1.43 | 2.27 | 0.12 | 1.46 | 1.07 | 4.00 | 1.43 | 4.61 |
| 100 | 1.82 | 2.89 | 0.14 | 1.49 | 1.09 | 8.00 | 1.58 | 5.10 |

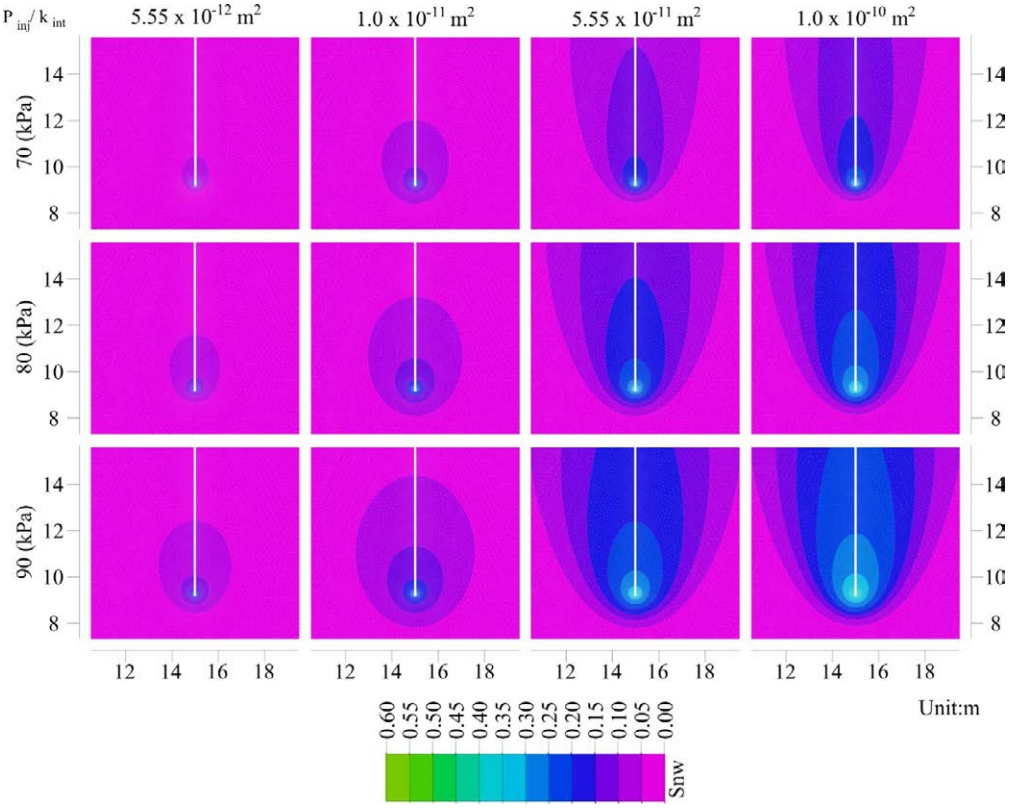


**Figure 7** Isocountors of $S_{nw}$ as a function of $P_{nw,inj}$ at $t = 1800s$. Distance in meters

of the desaturation zone. A similar behaviour is observed at all levels of injection pressures (70, 80, and 100 $kPa$), suggesting the existence of a maximum desaturation radius for a given injection pressure. The maximum value of $R_{eff}$ is reached more rapidly as the intrinsic permeability of the soil increases.

**Table 6** Summary of results obtained for $R_{eff}$ as a function of four different soils

| Soil | $k_{int}(m^2)$ | $R_{eff}(m)$ | $R_{eff}/R_0$ |
|---|---|---|---|
| 1 | $5.5x10^{-12}$ | **0.75** | 1.00 |
| 2 | $1.0x10^{-11}$ | 1.43 | 1.91 |
| 3 | $5.5x10^{-11}$ | 1.80 | 2.40 |
| 4 | $1.0x10^{-10}$ | 1.80 | 2.40 |

## 4. Conclusions

The following conclusions are drawn from the numerical simulations:

- Predictions are conducted to observe the suitability of the proposed model as a numerical tool that allows the in-situ desaturation front to be tracked. Consequently, it is shown that the numerical model presented in this work is appropriate to evaluate field desaturation processes when the material and hydraulic parameters of the soil are known.

- The injection pressure and soil's intrinsic permeability are the main factors affecting the effective radius of advance, $R_{eff}$. For a fixed time, $R_{eff}$ varies significantly with variations of $P_{nw,inj}$. For a fixed injection pressure, the increase in $R_{eff}$ is more pronounced at the beginning of the desaturation process and it becomes less marked as time advances. The threshold value is reached more rapidly when the intrinsic permeability increases. For all analysed cases, the soil trended to achieve a maximum $R_{eff}$ for a given pressure. For practical applications, and if a soil desaturation technique is intended, the value of $R_{eff}$ will serve to define the horizontal separation of injection wells and vertical separation of the injection points that have to be implemented for a particular project.

- It is observed that for a particular injection pressure, the more permeable the soil, the greater the *nw* phase front infiltration; in other words, the greater the advance of the desaturation plume within the saturated soil medium. For the most permeable soils, $k_{int} = 5.55x10^{-11}m^2$ and $1.00x10^{-10}m^2$, the increase in $R_{eff}$ is more pronounced as pressure increases. Both soils experience a similar effective

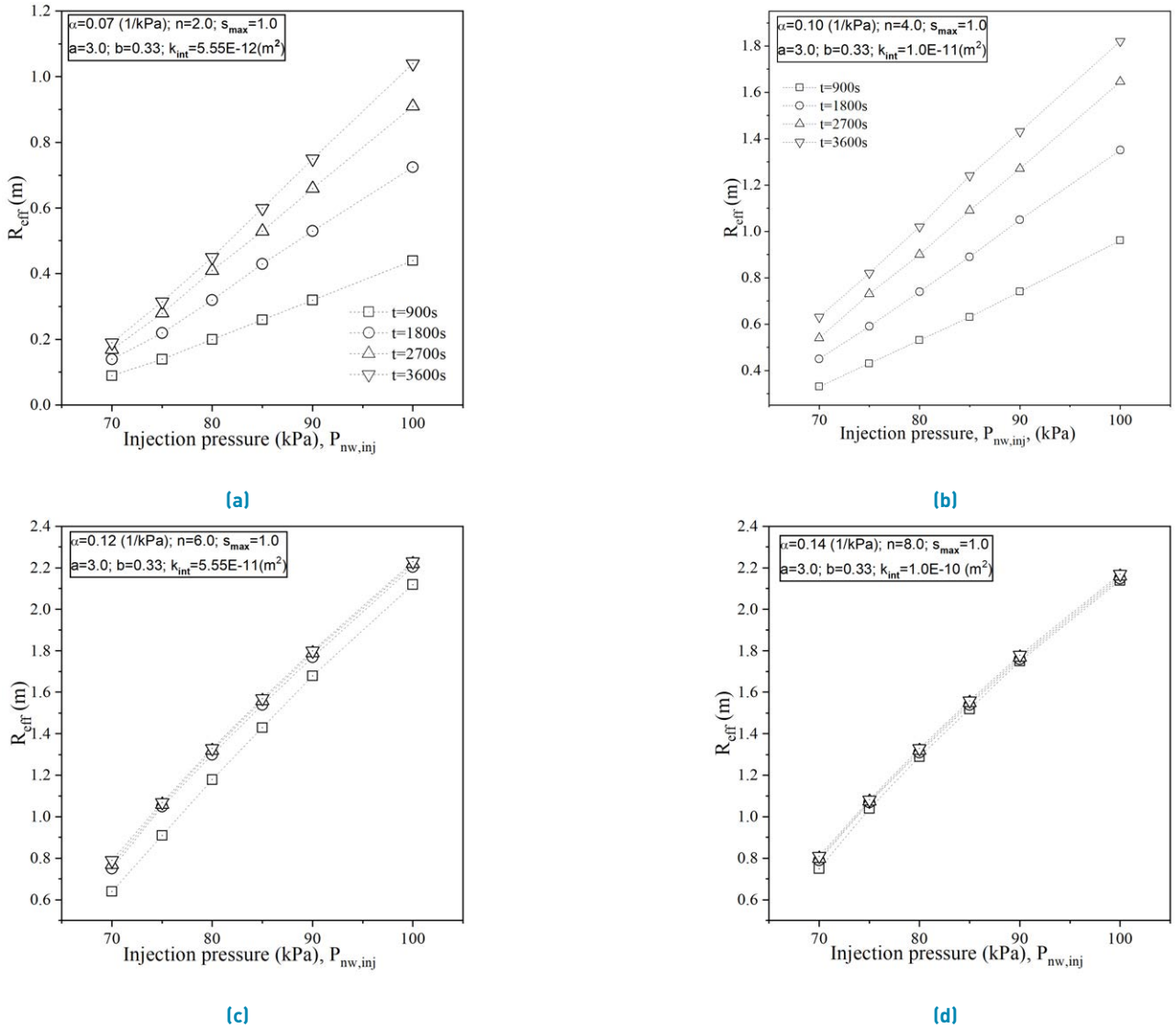


**Figure 8** $R_{eff}$ for soils shown in Table 3. *Snw*=0.1 and *Pnw,inj* from 70 to100 *kPa*

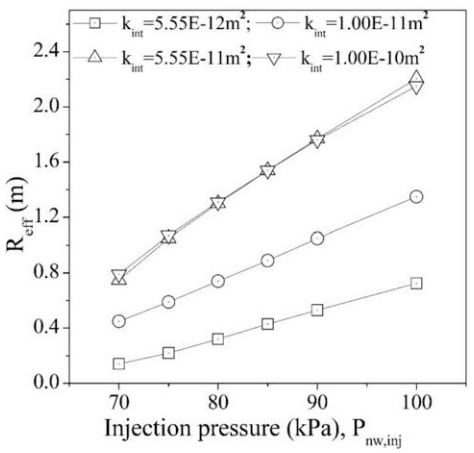


**Figure 9** $R_{eff}$ for *Snw*=0.1 and *Pnw,inj* from 70 to 100 *kPa* at *t*=1,800 *s*

radius regardless of the injection pressure, indicating that for a given pressure and as the soil's intrinsic permeability increases, there exists a threshold value for $R_{eff}$.

- For a fixed soil's intrinsic permeability and injection pressure, soil-water retention characteristic curve parameters ($\alpha$ and *n*) have a more significant influence on $R_{eff}$ than material parameters $a$ and *b* (permeability functions). $R_{eff}$ substantially increases as *n* increases (nonlinear response), implying that the shape of the soil-water retention curve has a significant effect on the advance of the desaturation front. $R_{eff}$ grows very rapidly, rapid transition from a saturated state to an unsaturated state, as the soil becomes coarser. Material parameters $a$ and *b* do not have a significant influence on $R_{eff}$ during air injection.

- The limitations and practical use of the findings presented in this study are encompassed within the framework of the unsaturated soil mechanics. The temperature effect and compressibility of phases were not included. The effects of some features of the gas bubble (e.g., type, pressure, size), injector (e.g., diameter, spacing), and mode of air injection (e.g., continues or pulsed) are out of the scope of this work and will be the subject of a future study.

## 5. Declaration of competing interest

We declare that we have no significant competing interests including financial or non-financial, professional, or personal interests interfering with the full and objective presentation of the work described in this manuscript.

## 6. Author contributions

Sebastián Sepúlveda-Cano: Conceptualization, Methodology, Investigation, Numerical Analysis, Data Analysis. Carlos A. Vega-Posada: Conceptualization, Methodology, Investigation, Supervision. Edwin F. García-Aristizábal: Conceptualization, Methodology, Investigation, Supervision.

## 7. Acknowledgements

The research presented in this paper was carried out at the University of Antioquia in Medellin, Colombia. The authors want to express their appreciation to the Infrastructure Research Group (GII) of the University of Antioquia for their support and suggestions.

## 8. Funding

The author(s) received no financial support for the research, authorship, and/or publication of this article.

## 9. Data availability statement

The authors confirm that the data supporting the findings of this study are available within the article.

## References

[1] R. B. Seed, K. O. Cetin, R. E. S. Moss, A. M. Kammerer, J. Wu, and *et al.*, "Recent advances in soil liquefaction engineering: A unified and consistent framework," in *Proceedings of the 26th Annual ASCE Los Angeles Geotechnical Spring*, Long Beach, CA, 2003, pp. 1–72.

[2] J. T. Dejong, K. Soga, E. Kavazanjian, S. Burns, and L. A. Van, "Biogeochemical processes and geotechnical applications: progress, opportunities and challenges," *Géotechnique*, vol. 63, no. 4, Mar. 2013. [Online]. Available: https://doi.org/10.1680/geot.SIP13.P.017

[3] P. Gallagher, A. Pamuk, and T. Abdoun, "Stabilization of liquefiable soils using colloidal silica grout," *Journal of Materials in Civil Engineering*, vol. 19, no. 1, Jan. 01, 2007. [Online]. Available: https://doi.org/10.1061/(ASCE)0899-1561(2007)19:1(33)

[4] M. Ishihara, M. Okamura, and T. Oshita, "Desaturating sand deposit by air injection for reducing liquefaction potential," in *2003 Pacific Conference on Earthquake Engineering*, Tsukuba, JA, 2003, pp. 1–6.

[5] M. Okamura and Y. Soga, "Effects of pore fluid compressibility on liquefaction resistance of partially saturated sand," *Soils and Foundations*, vol. 46, no. 5, Oct. 2006. [Online]. Available: https://doi.org/10.3208/sandf.46.695

[6] M. K. Yegian, E. Eseller-Bayat, A. Alshawabkeh, and S. Ali, "Induced-partial saturation for liquefaction mitigation: Experimental investigation," *Journal of Geotechnical and Geoenvironmental Engineering*, vol. 133, no. 4, Apr. 2007. [Online]. Available: https://doi.org/10.1061(ASCE)1090-0241(2007)133:4(372)

[7] E. E. Eseller-Bayat, M. K. Yegian, A. Alshawabkeh, and S. Gokyer, "Liquefaction response of partially saturated sands. i: Experimental results," *Journal of Geotechnical and Geoenvironmental Engineering*, vol. 139, no. 6, Jun. 2013. [Online]. Available: https://doi.org/10.1061/(ASCE)GT.1943-5606.0000815

[8] J. He, J. Chu, V. Inavov, and L. Laloui, "Mitigation of liquefaction of saturated sand using biogas," in *Bio- and Chemo-Mechanical Processes in Geotechnical Engineering*, 2015, pp. 116–124.

[9] N. P. Marasini and M. Okamaru, "Numerical simulation of centrifuge tests to evaluate the performance of desaturation by air injection on liquefiable foundation soil of light structures," *Soils and Foundations*, vol. 55, no. 6, Dec. 2015. [Online]. Available: https://doi.org/10.1016/j.sandf.2015.10.005

[10] *FlexPDE 5 User Guide*, PDE Solutions Inc, 2005.

[11] G. F. Pinder and W. G. Gray. (2008) Essentials of multiphase flow and transport in porous media. Wiley Online Library. [Online]. Available: https://onlinelibrary.wiley.com/doi/book/10.1002/9780470380802

[12] H. Darcy, *Determination of the laws of flow of water through sand*. Physical hydrology, 1983.

[13] M. T. van Genuchten, "A closed-form equation for predicting the hydraulic conductivity of unsaturated soils," *Soil Science Society of America Journal*, vol. 44, no. 5, Sep-Oct. 1980. [Online]. Available: https://doi.org/10.2136/sssaj1980.03615995004400050002x

[14] P. Horgue, C. Soulaine, J. Franc, R. Guibert, and G. Debenest, "An open-source toolbox for multiphase flow in porous media," *Computer Physics Communications*, vol. 187, Feb. 2015. [Online]. Available: https://doi.org/10.1016/j.cpc.2014.10.005

[15] H. Yasuhara, M. Okamura, and Y. Kochi, "Experiments and predictions of soil desaturation by air-injection technique and the implications mediated by multiphase flow simulation," *Soils and Foundations*, vol. 48, no. 6, Dec. 2008. [Online]. Available: https://doi.org/10.3208/sandf.48.791

[16] B. Mao, Z. Liu, S. Liu, W. Fang, and Z. Chen, "Effects of soil property and air injection condition on airflow behavior during air sparging," *Fresenius Environmental Bullet*, vol. 26, no. 6, pp. 3942––3955, Dec. 2017.

[17] C. W. Fetter, T. Boving, and D. Kreamer, *Contaminant Hydrogeology*. Long Grove, IL: Waveland Press, INC, 2017.

[18] K. R. Reddy and J. A. Adams, "System effects on benzene removal from saturated soils and ground water using air sparging," *Journal of Environmental Engineering*, vol. 124, no. 3, Mar. 1998. [Online]. Available: https://doi.org/10.1061/(ASCE)0733-9372(1998)124:3(288)

[19] R. L. Johnson, P. C. Johnson, D. B. McWhorter, R. E. Hinchee, and I. Goodman, "An overview of in situ air sparging," *Groundwater Monitoring & Remediation*, vol. 13, no. 4, Nov. 1993. [Online]. Available: https://doi.org/10.1111/j.1745-6592.1993.tb00456.x/

[20] N. R. Thomson and R. L. Johnson, "Air distribution during in situ air sparging: an overview of mathematical modeling," *J Hazard Mater.*, vol. 72, no. 2-3, Feb. 2000. [Online]. Available: https://doi.org/10.1016/S0304-3894(99)00143-0

[21] P. D. Lundegard and D. LaBrecque, "Air sparging in a sandy aquifer (florence, oregon, u.s.a.): Actual and apparent radius of influence," *Journal of Contaminant Hydrology*, vol. 19, no. 1, Jul. 1995. [Online]. Available: https://doi.org/10.1016/0169-7722(95)00010-S

[22] N. Lu, "Unsaturated soil mechanics: Fundamental challenges, breakthroughs, and opportunities," *Journal of Geotechnical and Geoenvironmental Engineering*, vol. 146, no. 5, May 2020. [Online]. Available: https://doi.org/10.1061/(ASCE)GT.1943-5606.0002233

[23] J. C. aned J. Hopmans and M. Grismeru, "Parameter estimation of two-fluid capillary pressure–saturation and permeability functions," *Advances in Water Resources*, vol. 22, no. 5, Jan. 1999. [Online]. Available: https://doi.org/10.1016/S0309-1708(98)00025-6

[24] H. Ogata and M. Okamura, "Experimental study on air behaviour in saturated soil under air injection," in *Proc. Symp. On Natural Disaster Prevention, JSCE*, Tokushima, Japan, 2006, pp. 89–90.

[25] A. Zeybek and G. S. P. Madabhushi, "Durability of partial saturation to counteract liquefaction," in *Proceedings of the Institution of Civil Engineers-Ground Improvement*, London, UK, 2017, pp. 102–111.

[26] R. C. Chaney, "Saturation effects on the cyclic strength of sands," in *From Volume I of Earthquake Engineering and Soil Dynamics–Proceedings of the ASCE Geotechnical Engineering Division Specialty Conference*, Pasadena, CA, 1978, pp. 342–358.

[27] Y. Yoshimi, K. Tanaka, and K. Tokimatsuu, "Liquefaction resistance of a partially saturated sand," *Soils and Foundations*, vol. 29, no. 3, Sep. 1989. [Online]. Available: https://doi.org/10.3208/sandf1972.29.3_157

[28] M. Okamura, M. Takebayashi, K. Nishida, and N. Fujii, "In-situ desaturation test by air injection and its evaluation through field monitoring and multiphase flow simulation," *Journal of Geotechnical and Geoenvironmental Engineering*, vol. 137, no. 7, Jul. 2011. [Online]. Available: https://doi.org/10.1061/(ASCE)GT.1943-5606.0000483

[29] E. K. Nyer and S. S. Suthersan, "Air sparging: Savior of ground water remediations or just blowing bubbles in the bath tub?" *Groundwater Monitoring & Remediation*, vol. 13, no. 4, Nov. 1993. [Online]. Available: https://doi.org/10.1111/j.1745-6592.1993.tb00453.x

[30] M. R. Chen, R. E. Hinkley, and J. E. Killough, "Computed tomography imaging of air sparging in porous media," *Water Resources Research*, vol. 32, no. 10, Oct. 01, 1996. [Online]. Available: https://doi.org/10.1029/96WR01136

[31] K. R. Reddy, S. Kosgi, and J. Zhou, "A review of in-situ air sparging for the remediation of voc-contaminated saturated soils and groundwater," *Hazardous Waste and Hazardous Materials*, vol. 12, no. 2, Jan. 1995. [Online]. Available: https://doi.org/10.1089/hwm.1995.12.97